

Available online at www.sciencedirect.com

ScienceDirect

journal homepage: www.elsevier.com/locate/ije

Hydrogen adsorption in pyridine bridged porphyrin-covalent organic framework

Sarbani Ghosh*, Jayant K. Singh

Department of Chemical Engineering, Indian Institute of Technology, Kanpur, UP, India

ARTICLE INFO

Article history:

Received 27 August 2018

Received in revised form

6 November 2018

Accepted 10 November 2018

Available online 13 December 2018

Keywords:

Covalent organic framework

Porphyrin COF

Hydrogen storage

Adsorption

GCMC

DFT

ABSTRACT

Covalent organic frameworks (COFs), a class of carbon-based polymeric materials have the potential to be used as hydrogen adsorbent. Three dimensional (3D) COFs, due to their low density and high surface area, although have higher hydrogen adsorption, they have less stability than two dimensional (2D) COFs. Here we studied porphyrin group containing 2D COF, namely H₂P-COF for hydrogen storage using density functional theory (DFT) and grand canonical Monte Carlo (GCMC) simulations and the results were compared with the most common 2D COFs, COF-1 and COF-5. Cylindrical shaped 2D COFs where isolated unit blocks are stacked in multiple layers due to van der Waals interactions between individual layers, increase the effective surface area for hydrogen storage. A further modification has been done by bridging the inter-layer gap by pyridine molecules. Insertion of pyridine increases the separation distance of layers of 2D COFs as well as the free volume. Feasibility of the structure formation and stability of all the structures were checked using DFT study. To ensure the structural stability of bridged COFs after hydrogen loading, alternating layers of COF were bridged. Single, bi, tri and tetra -pyridine molecules were chemically bonded with the existing carbon ring present in between two C₂O₂B rings to form pyridine bridged H₂P-COFs. Our GCMC results show a significant increase in storage capacity which is mainly due to an increase in the free volume of the material. The highest capacity of ~ 5.1 wt% and 20 g H₂/L at 298 K and 100 bar, above the gravimetric DOE goal, has been found at room temperature for tetra-pyridine doped porphyrin COF structure.

© 2018 Hydrogen Energy Publications LLC. Published by Elsevier Ltd. All rights reserved.

Introduction

The increased rate of our energy consumption and extreme environment pollution forced us to be focused on the replacement of fossil fuels by alternative energy. The alternative source of energy should be abundant, renewable, cheap and definitely be clean. Considering all the facts, hydrogen has the potential to be a perfect alternative to fossil fuels. Although hydrogen is a widely available source of energy, is

mainly available as hydrocarbons or other hydro-compounds. Thus, molecular hydrogen needs to be derived from various sources. The commercial technique of hydrogen production, burning of fossil fuels is being replaced by biomass gasifications, solar electrolysis and wind electrolysis [1]. Wide commercialization of hydrogen-based fuel cell where hydrogen burns in presence of oxygen and produces non-polluting water vapour, is undeployed mainly due to lack of effective storage of this low density gas at ambient conditions. Compared to all the convenient storage processes, storage in

* Corresponding author.

E-mail address: sarbani.ghosh.chemical@gmail.com (S. Ghosh).

<https://doi.org/10.1016/j.ijhydene.2018.11.066>

0360-3199/© 2018 Hydrogen Energy Publications LLC. Published by Elsevier Ltd. All rights reserved.

terms of adsorbed molecular hydrogen in a solid adsorbent e.g., carbonaceous materials, polymeric materials, metal organic frameworks, zeolites, is a safe and energy efficient process. This storage is mainly driven by weak van der Waals interactions between the hydrogen molecules and the adsorbent. Thus, to achieve a high storage value, large surface area of the adsorbent, high accessible pore volume and a strong van der Waals interactions towards H_2 are desired. The minimum criterion of storage is such that the vehicle driven by hydrogen needs 3.1 kg of hydrogen for 500 km of driving. The U.S. Department of Energy (DOE) has defined a standard technique to quantify the storage amount based on gravimetric density and volumetric density with a storage target of 4.5 wt% and 30 g/L, to be reached by the year 2020 at a temperature range of 233–333 K [2,3]. Adsorption of hydrogen gas molecules in light-weight carbonaceous materials is found to be promising to reach the DOE storage target. Carbon-based nanomaterials have gained substantial attention [4], as the structures are entirely or mainly formed from lightweight aromatic carbon rings, possesses high thermal stability (up to ~ 5000 K), have wide tunable structure properties and resistance towards humidity, hence are useful in domestic and mobile application. Although the carbonaceous materials like carbon nanotubes, nanoscrolls, graphene etc. were found to be promising at low temperature (~ 77 K), at room temperature the efficiency is still very low. The previous study of beryllium and titanium -doped defective carbon nanotube, shows that the storage capacity above the storage goal can be reached at room temperature and a high pressure of ~ 245 – 350 atm [5,6]. However, metal organic frameworks (MOFs) have excellent storage capacity near ambient conditions due to their high density of free volume, high active surface area and high tunability but are challenging to commercialize in large scale as most of the MOFs don't have resistance in humid environment. In this regards, carbon-based materials are proven to be easily commercialized, but an appropriate carbon-based adsorbent for hydrogen storage is yet way off to be commercialized. In recent years, Yaghi and co-workers synthesized a new generation of carbon-based crystalline porous structure, named as covalent organic frameworks (COFs) which could be capable of ambient hydrogen storage. The strong covalent bonds of COF make it stable, and the light-weight elements (such as C, B, N, O, H, Si) of COFs make it appropriate for the mobile application by not increasing the weight of the material. Like other carbonaceous structures, they are porous, thermally stable (upto ~ 800 K [7]), tunable and ordered, and hence, is easy to commercialize. The COFs can mainly be categorized as two dimensional (2D) and three dimensional (3D) COF. In 2005, two dimensional (2D) COFs were first formed by Côté et al. [7] through a condensation reaction of boronic acid at ~ 358 – 393 K. After two years, consequently 3D COFs were formed by the same group [8]. Theoretically and experimentally COF structures have been used to study hydrogen adsorption in the past. The reported excess storage capacity of COF-1 at 77 K and 1 atm is 1.28 wt% and at room temperature and 100 bar is 0.26 wt% [9]. 3D COFs have higher capacity to store hydrogen [10,11] compared to 2D COFs due to the larger pore volume of 3D COFs. Among the 3D COFs, COF-108 has the highest gravimetric capacity of 18.9 wt % and COF-105 has the highest volumetric capacity of 40 gH_2/L

at cryogenic temperature of 77 K. Assfour and Seifert in 2010 [12] reported that 3D COFs, COF-105 and COF-108 although have the highest hydrogen storage capacities, have the lowest stability with bulk module value of 3.33 GPa and 0.05 GPa, respectively. On the other hand, 2D COF, COF-1 has highest heat of adsorption [10], hence have a potential for ambient hydrogen storage. Although 3D COFs have exceptional storage capacities at low temperature of 77 K, storage of hydrogen near ambient conditions is more desirable concerning the practical application. Doping of COFs provides an additional binding states for hydrogen molecules [13]. Substitutional doping can increase the binding energy where doping by joining bonds with existing atoms can also increase the available surface area. 3D COFs, COF-105 doped with lithium alkoxide groups [14], COF-108 doped with Mg_2N [15] and COF-301 doped with $PdCl_2$ [16] reached the storage capacity of 6 wt %, 2.73 wt% and 4.2 wt%, respectively at 298 K. A high accessible surface area is the major limiting factor for COF structures to increase the gravimetric storage. As the surface area reduces, accessing all the binding states due to steric repulsion will become difficult, leading to decrease in the gravimetric capacity. Boron atom present in COF-1 can behave like Lewis acid to react with pyridine base and insertion of pyridine in COF-1 increases the hydrogen uptake by increasing the accessible surface area [17]. Palladium metal has a strong attraction towards hydrogen molecule [18], thus doping of $PdCl_2$ on COF-301 increases hydrogen uptake and at room temperature and it reaches the volumetric DOE storage target [16] but on the other hand, failed to reach the gravimetric target which might be due to the heavy atomic mass of Pd atom. A recent study showed that one Sc atoms doped on $(C_6H_3)_2(B_2C_4H_4)_3Sc_6$ COF increases the binding energy upto ~ 3.4 eV and able to bind 24 H_2 molecules [19]. The predicted gravimetric storage capacity of $(C_6H_3)(B_2C_4H_4)_3Sc_6$ COF is ~ 7.0 wt%. A newly designed porphyrin covalent organic polyhedra also showed promising storage capacity at 77 K [20].

All the above studies state that modification of COFs can enhance the storage capacity at room temperature. Here, we chose 2D COFs for further modification due to their more stability and ease of formation compared to 3D COFs. COF-1, COF-5 from the study of Côté et al. [7] are used as base structures to compare our new study. Porphyrin group included H_2P -COF [21] is used for the first time to check hydrogen storage capacity. Nitrogen-containing COFs are more chemically stable upon exposure to moisture thus porphyrin group present in COF increases the stability due to the more stable C-N bond [22,23]. 2D COFs have graphene like structures, and they can be further stacked to form a cylindrical tube like structures [24,25]. COF-1 consists of hexagonal boroxine ($B_3H_3O_3$) ring and hexagonal benzene rings can be stacked in multiple layers with a separation distance of 3.46 Å [7]. COF-5, where the building block is triboronate ester was also formed in the same way as COF-1, by self-condensation reaction of boronic acid and hexahydroxy triphenylene (HHTP) at a temperature of ~ 358 K. The main difference in COF-1 and COF-5 is that COF-1 consists of hexagonal B_3O_3 rings and COF-5 consists of pentagonal C_2O_2B rings along with hexagonal carbon rings. In this work, we have investigated the hydrogen storage in COF structures using molecular simulation. In particular, we have used isolated 2D COFs in x and y

directions and found that the isolated one unit of 2D COFs, stacked in multiple layers in z direction by forming cylindrical shape has higher hydrogen storage capacity compared to the planar structure. In order to further increase the effective surface area, we increase the interlayer spacing by bridging of pyridine molecule. B, N, S present in COFs can act as a Lewis acid to attach with Lewis base like pyridine which also increases the stability of COFs [26]. The pyridine ring can also be possible to attach with carbon atoms present in COF (Tilford et al. [26] suggested the possible functionalized position in COFs). As the pyridine molecule shows polymerization characteristic [27,28] and bi-pyridine molecule also does exist, we doped the COF with bi-pyridine, tri-pyridine, tetra-pyridine molecules in between two adjacent layers which increases the interlayer spacing. Bridging pyridine molecules in 2D COFs shows significant improvement in hydrogen storage capacity.

The rest of the paper is organized as follows: In models and methods section we describe the construction of the pyridine bridged COF and the simulation details including density functional theory (DFT) and grand canonical Monte Carlo (GCMC) simulations. Next, in the result section, we first describe the structural properties obtained from DFT calculations and Voronoi tessellation, followed by GCMC results. In GCMC results we mainly describe the hydrogen adsorption in tubular shape COFs. A small comparison of tubular COFs with planar COFs are available in Supplementary Information [A]. Finally, we conclude the paper with a brief overview.

Models and methods

We arranged unit blocks of two dimensional COFs in AA stacking (without any translation in x and y directions between individual layers) at their respective equilibrium spacing (in z direction) to give a tubular shape as inspired by Pachfule et al. and Karak et al. [24,25]. If it is possible to isolate a unit block of COF as shown in Table 1, tubular COF can be formed (as shown in Fig. 1b) which slightly increases the storage capacity. COF-1, COF-5, H₂,P-COF were studied as tubular COF and also compared with planar structures in Supplementary Information [Appendix A]. In planar COF structures, the structure will be spanned in x, y direction instead of one block to form a sheet like structure, as shown in Fig. 1a. Pyridine doped porphyrin COF structures were formed by adding pyridine molecules to C-atom present in COF. To build one pyridine bridged H₂,P-COF (1-P), one pyridine molecule was attached to the carbon ring which is present in between two C₂O₂B rings. H₂,P-COF has four pairs of C₂O₂B ring, as shown in Table 1. Thus in 1-P, H₂,P-COF, total four pyridine molecules are present in between two adjacent layers. Alternative layer bridged COF (a-bridged) was formed by adding pyridine molecules between 1st and 2nd layer and then between 3rd and 4th layer by leaving 2nd and 3rd layers as un-doped at the equilibrium spacing. Subsequently, 2-P, 3-P and 4-P, H₂,P-COFs were formed by increasing the number of pyridine molecule attached to each carbon ring from one to two, three and four, respectively. Multiple layers of COF were taken to stack them and to form ~ 40 Å long tube, as shown in Fig. 2. In Fig. 2, one pyridine molecule and four pyridine molecules -doped COFs are shown and all the other COF

structures are shown in Supplementary Information [Appendix A] (see Fig. S1 and Fig. S2).

DFT study

In order to efficiently design pyridine bridged porphyrin COF structures, we performed density functional theory (DFT) calculations. To check the energetic stability and feasibility of the predicted structures we optimized all the COF structures using DFT calculation as implemented in Quantum-Espresso which is based on plane-wave basis set [29]. Second-order Moller–Plesset level of theory (MP2) [14] and Perdew–Wang 91 (PW-91) DFT level with generalized gradient approximation (GGA) [13,15,23] are widely used for COFs. In our calculation, we optimized two layers of COF-1 in two different ways by using GGA DFT of PW-91 exchange–correlation functional and local density approximation (LDA) DFT of Perdew–Zunger (PZ) exchange–correlation functional. GGA DFT with PW-91 exchange–correlation functional predicts that the interlayer spacing of COF-1 is 3.46 Å, which is comparable with the experimentally reported value [7]. Afterwards, we used GGA of PW-91 to perform all the DFT calculations. Ultra-soft pseudo-potential, taken from the Quantum-Espresso library for all the atoms, was used to solve the Kohn–Sham equation. The system was periodic in x, y, z directions with minimum vacuum distance of ~ 10 Å. After optimizing two layers of 2D COFs and calculating inter-layer spacing, only one periodic building block as shown in Fig. 3 was considered for modification of COFs and for further calculations. Kinetic energy cut-off of ~ 816 eV (60 Ry) and charge density cut-off of 4082 eV (300 Ry) were used. Due to the large system size, only gamma points were considered. Broyden–Fletcher–Goldfarb–Shanno (BFGS), a quasi-Newton algorithm was used for structure relaxation and the forces acting on each atom were computed by Hellmann–Feynman theorem. All the structures were fully optimized until the forces acting on each ion became less than 0.003 eV/atom, the change in total energy between two consecutive steps became less than 0.0001 eV.

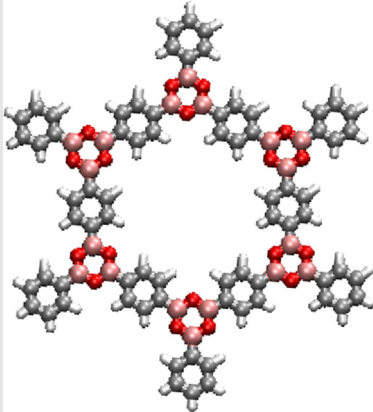
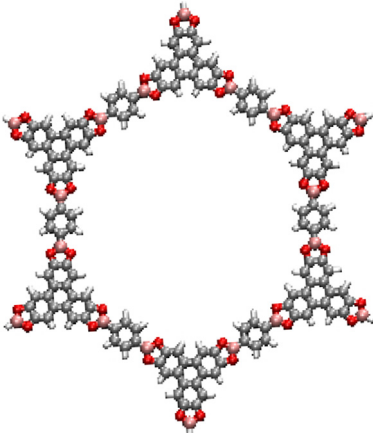
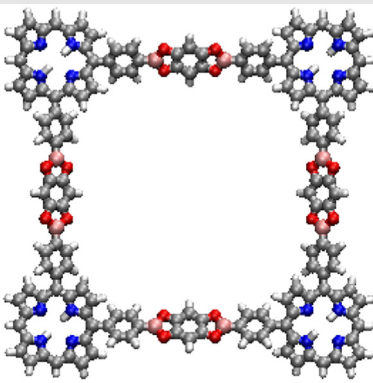
GCMC simulations

Grand canonical Monte Carlo (GCMC) simulations were used to study theoretical hydrogen uptake of COFs using LAMMPS package [30]. Atomistic (all-atom) model was used to describe both hydrogen molecules and COF structures. COF structures were placed in the center of a periodic box ($x = y = 100$ Å) as rigid such that the center of mass of the COF always remains at the center of the box. GCMC simulations were carried out with the following moves with equal probability:

- insertion of new H₂ molecules inside the system,
- deletion of existing H₂ molecules,
- translation and rotation of existing H₂ molecules.

Thus, we select an empty structure, and eventually, for a given chemical potential a mean number of hydrogen molecules is populated. Periodic boundary conditions were applied in all the three directions. In the case of isolated tubular COF structures (see Fig. 1b) where the tube is infinitely periodic in z direction, outside surface adsorption is also possible. The van

Table 1 – Single unit of 2D COFs used in this study.

Name	D (Å) ^a	d (Å) ^b	unit block ^c
COF-1	15	3.46	
COF-5	27	4.52	
H ₂ P-COF	25	3.9	

^a D is the diameter of COF.

^b d is the equilibrium inter-layer spacing between two adjacent COF layers.

^c Carbon, oxygen, boron, nitrogen, and hydrogen atoms are shown in grey, red, pink, blue, and white colours, respectively.

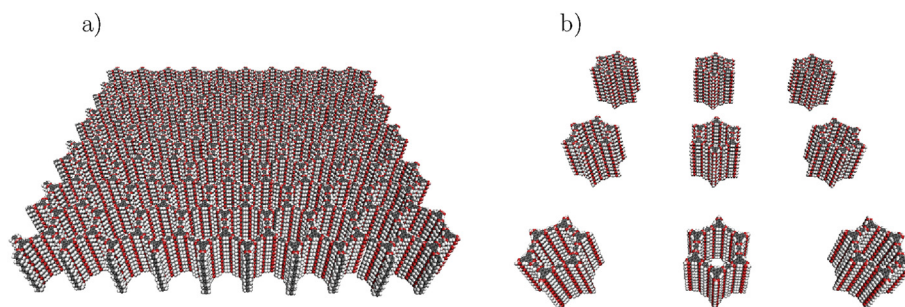


Fig. 1 – a) Planar COF structure where it is spanned in x, y and z directions to form a sheet like structure and b) Tubular COF structures where the COF is finite in x and y direction and spanned in z direction to form isolated tube like structure. Carbon, oxygen, boron, nitrogen, and hydrogen atoms are shown in grey, red, pink, blue, and white colours, respectively. (For interpretation of the references to color in this figure legend, the reader is referred to the Web version of this article.)

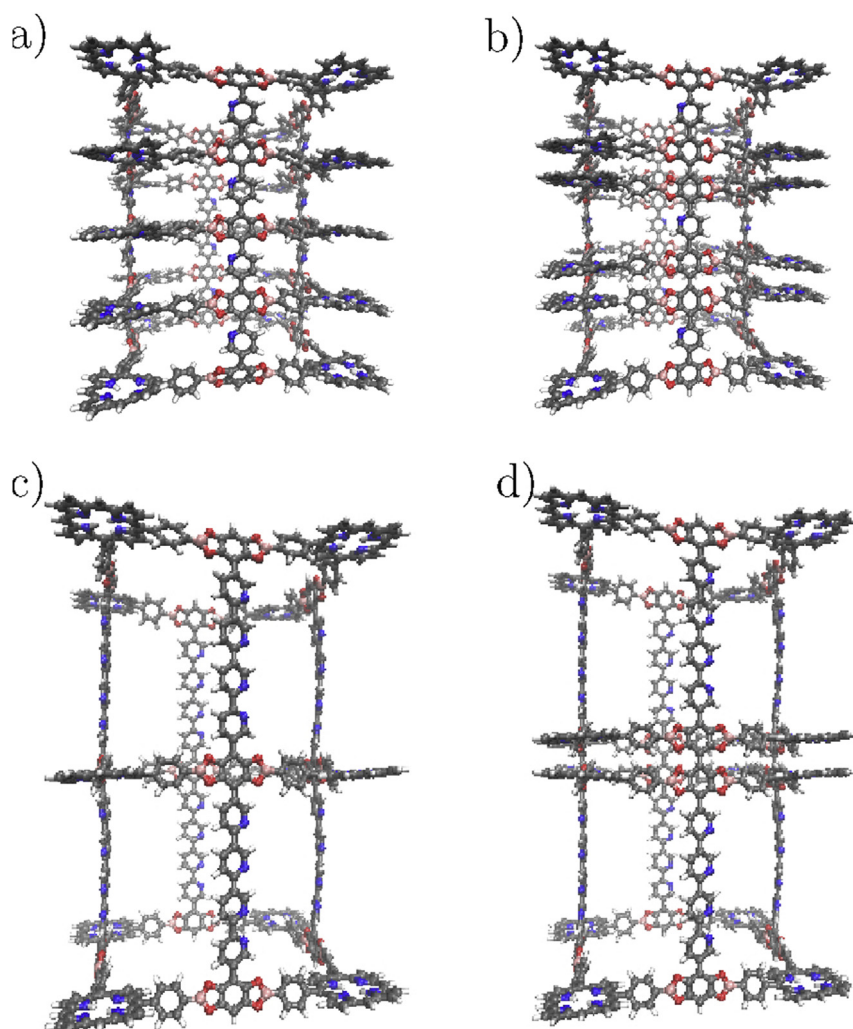


Fig. 2 – Tubular pyridine doped porphyrin COF structures: a) single pyridine molecule consecutive doped COF [1-P, H₂,P-COF], b) single pyridine molecule alternative doped COF 1-P [H₂,P-COF (a-bridged)], c) tetra pyridine molecule consecutive doped COF [4-P, H₂,P-COF] and d) tetra pyridine molecule alternative doped COF [4-P, H₂,P-COF (a-bridged)]. Carbon, oxygen, boron, nitrogen, and hydrogen atoms are shown in grey, red, pink, blue, and white colours, respectively. (For interpretation of the references to color in this figure legend, the reader is referred to the Web version of this article.)

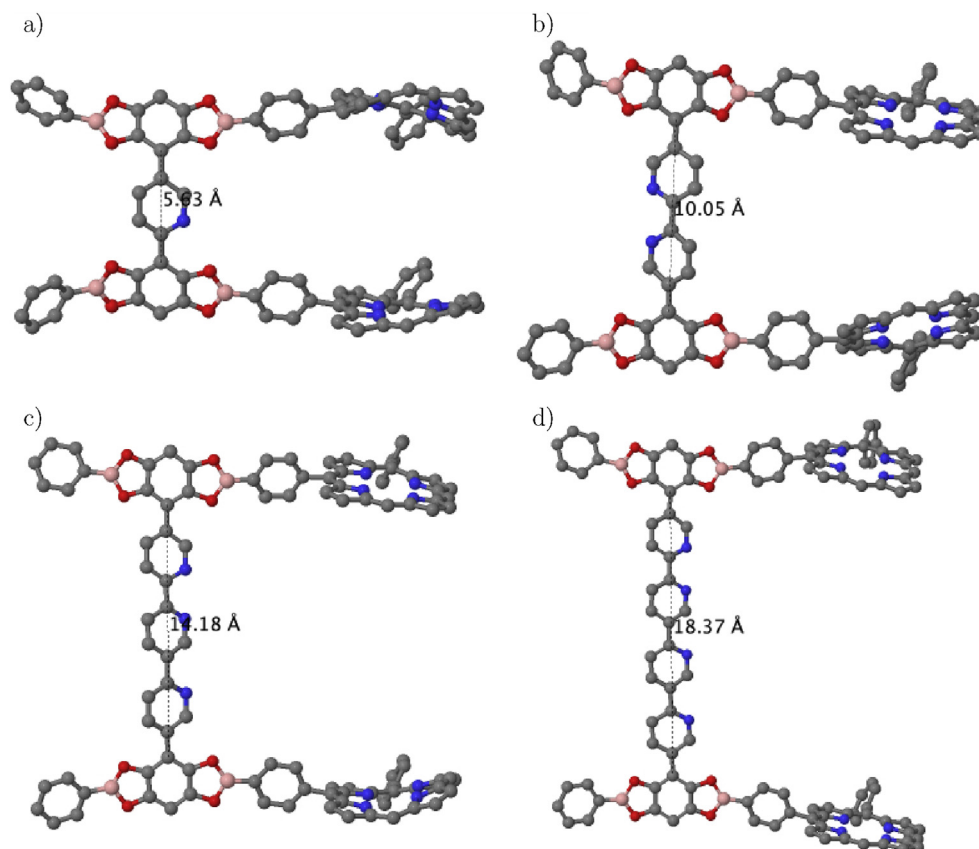


Fig. 3 – DFT optimized structures of pyridine bridged H₂P-COF, where a) 1-P, H₂-PCOF, b) 2-P, H₂-PCOF, c) 3-P, H₂-PCOF and d) 4-P, H₂-PCOF. Carbon, oxygen, boron and nitrogen atoms are shown in grey, red, pink, and blue colours, respectively. Hydrogen atoms are not shown for clarity. (For interpretation of the references to color in this figure legend, the reader is referred to the Web version of this article.)

der Waals interactions between H₂ and COFs were defined in this study using Morse force-field (FF) as the theoretical uptake simulated by the potential are in good agreement with experimental hydrogen adsorption in COF structures [10,11,16,31]. The bulk density of hydrogen gas molecules calculated using the particular FF is close to the experimental data (shown in Fig. S3) and also comparable with OPLS-AA [32] force-field (shown in Table S1). Interaction energy ($V_{ij}^{morse}(r)$) for Morse potential are calculated using Eq. (1) and the parameters are tabulated in Table 2. Here, the total potential energy is the only contribution of non-bonded van der Waals energy as it is proven to dominate the hydrogen adsorption [33]. The potential was switched off smoothly at a distance of 15 Å.

$$V_{ij}^{morse}(r) = D_0 \left[e^{-2\alpha(r_{ij}-r_0)} - 2e^{-\alpha(r_{ij}-r_0)} \right] \quad (1)$$

where, D_0 is the energy well-depth, r_0 is the equilibrium distance between two species and α is the force constant.

Temperature (T) was fixed at 298 K and hydrogen isotherms were calculated by varying the pressure (P) from 1 bar to 100 bar. The system was equilibrated for 100000 GCMC steps and 500000 consecutive steps were run to collect the data for analysis. In GCMC simulations, the chemical potential (μ) of hydrogen gas was fixed according to reservoir pressure (P).

Table 2 – Non-bonded forcefield parameters of hydrogen and COFs.

Morse force field			
Species ^a	D_0 (kcal/mol)	α (1/Å)	r_0 (Å)
H-C	0.10082	1.92	3.12
H-B	0.04825	1.51	3.49
H-O	0.02515	1.81	3.22
H-H1	0.00087	1.85	3.25
H-N	0.02940	1.55	3.25
H-H	0.01815	1.50	3.57

^a H is the hydrogen atom of hydrogen molecule, H1 is the hydrogen atom which is attached with COFs and all the other symbols has it's usual meaning.

The pressure was corrected by the fugacity coefficient (ϕ) and ϕ is calculated using Eq. (2a–d) from the study of Luo et al. [34].

$$\ln \phi = c_1 P - c_2 P^2 + c_3 [\exp(-P/300) - 1] \quad (2a)$$

$$c_1 = \exp(-3.8402T^1/8 + 0.5410) \quad (2b)$$

$$c_2 = \exp(-0.1263T^1/2 - 15.980) \quad (2c)$$

$$c_3 = 300\exp(-0.11901T - 5.941) \quad (2d)$$

Chemical potential is then calculated using Eq. (3)

$$\mu = kT \ln \frac{\phi P \Lambda^3}{kT} \quad (3)$$

where, k is the Boltzman's constant, T is the temperature and Λ is the thermal de-Broglie wavelength used as a dimensional consistency constant, set to 1.

Results and discussion

All the structures, used in this study were optimized by DFT calculations. Optimized building blocks of pyridine doped porphyrin COFs are shown in Fig. 3. Addition of pyridine molecules increases the inter-layer spacing from the equilibrium value of 3.9 Å up to ~ 18.37 Å.

Formation energies (E_{form}) were calculated to check the feasibility of the formation of pyridine doped COF structures using Eq. (4).

$$E_{form} = \frac{E_{n-P,COF} - E_{COF} - N_P \times \mu_P}{N} \quad (4)$$

where, $E_{n-P,COF}$ is the energy of the pyridine-doped COF with $n = 1, 2, 3$ and 4 , E_{COF} is the energy of the two layers of COF placed at equilibrium inter-layer spacing, μ_P is the chemical potential of the pyridine molecule, N_P is the number of pyridine molecule doped in COF, and N is the total number of atoms. μ_P is calculated from the Open Quantum Materials Database (OQMD) where the chemical potentials of the elements are fitted to experimental values in order to accurately predict the formation energy [35,36]. The values are tabulated in Table 3. The negative values indicate thermodynamic favourability of the structures to be formed. We note as the absolute values of E_{form} are increasing with increasing the number of pyridine molecules, the process of increment in the number (n) is spontaneous. Cohesive energy which defines how the atoms are bonded to a particular structure was calculated using Eq. (5). It was calculated from DFT energies and also from experimentally fitted chemical potentials of the elements (see Table 3).

Table 3 – Properties of Pyridine Bridged P-COF Calculated from DFT calculations.

COF	d (Å) ^a	E_{coh}^0 (eV) ^b	E_{coh}^μ (eV) ^b	E_{form} (eV) ^b	Element	μ (eV) ^c
0-P	3.90	-5.681	-8.710	–	H	-3.394
1-P	5.63	-5.763	-8.791	-6.026	B	-6.678
2-P	10.05	-5.763	-8.773	-11.458	C	-9.217
3-P	14.18	-5.754	-8.756	-16.354	N	-8.122
4-P	18.37	-5.765	-8.741	-20.825	O	-4.485

^a d is the interlayer spacing.

^b E_{coh} , E_{form} are cohesive and formation energy, respectively.

^c The chemical potential (μ) of the elements used in this study was taken from experiment.

Table 4 – Theoretically calculated properties of COFs used in this study.

(a) Unmodified COFs				
Name ^e (unmodified)	S_{acc} ^a (m ² /g)	V_{acc} ^b (cm ³ /g)	V_f ^c	ρ_{COF} ^d (g/cm ³)
COF-1	1801.23	0.334	0.266	0.795
COF-5	2654.16	1.047	0.5096	0.486
H ₂ P-COF	1275.94	0.291	0.258	1.581
(b) Modified COFs				
H ₂ P-COF (bridged)	S_{acc} (m ² /g)	V_{acc} (cm ³ /g)	V_f	ρ_{COF} ^d (g/cm ³)
1-P	4373.06	0.940	0.4604	0.490
2-P	4838.47	1.510	0.5596	0.370
3-P	4594.23	1.973	0.635	0.321
4-P	4866.91	2.457	0.6846	0.278
H ₂ P-COF (a-bridged) ^f	S_{acc} (m ² /g)	V_{acc} (cm ³ /g)	V_f	ρ_{COF} ^d (g/cm ³)
1-P	3418.31	0.876	0.4632	0.528
2-P	3999.70	1.170	0.513	0.438
3-P	3975.07	1.682	0.609	0.377
4-P	4270.47	2.116	0.6592	0.311

^a S_{acc} is the accessible surface area.

^b V_{acc} is the accessible pore volume for H₂ with probe radius of 1.36 Å.

^c V_f is the fraction of free volume for H₂.

^d ρ_{COF} is the accessible void density of COF for H₂.

^f 'a-bridged' COFs are alternate pyridine bridged COFs.

^e S_{acc} , V_{acc} & V_f of unmodified tubular COFs and pyridine bridged modified COFs are calculated.

$$E_{coh}^0 = \frac{E_{total} - \sum_{x=C,B} N_x E_x}{N} \quad (5a)$$

$$E_{coh}^\mu = \frac{E_{total} - \sum_{x=C,B} N_x \mu_x}{N} \quad (5b)$$

where, E_{total} is the total energy of pyridine doped COF, N_x , E_x and μ_x are the numbers, energy and chemical potential of atom x , respectively with $x = \text{carbon, boron, nitrogen, oxygen, hydrogen}$. Higher absolute values indicate higher chemical stability since more energy is required to detach atoms from the structure. Very negligible difference in the E_{coh} values represents almost equal chemically stable structures are formed. Binding energies (E_b) for H₂ molecule were calculated using Eq. (6).

$$E_b = E_{COF+H_2} - E_{COF} - E_{H_2} \quad (6)$$

where, E_{COF+H_2} is the total energy of H₂ placed COF structures, E_{COF} is the energy of COF structure without H₂ molecule and E_{H_2} is the energy of the H₂ molecule. Optimum adsorption site for one H₂ molecule was calculated by placing the molecule on top of one carbon ring, one boron containing ring, one pyridine molecule and on top of one porphyrin group. The adsorption sites and the respective binding energies are shown in Fig. 4. The highest value of E_b is when the hydrogen is placed on top of C₂O₂B ring. Thus the pentagonal boron containing ring is favoring the hydrogen adsorption. The porphyrin group has the second most hydrogen adsorption favorability. Although the pyridine molecule has the least adsorption energy compared to others, the molecules are

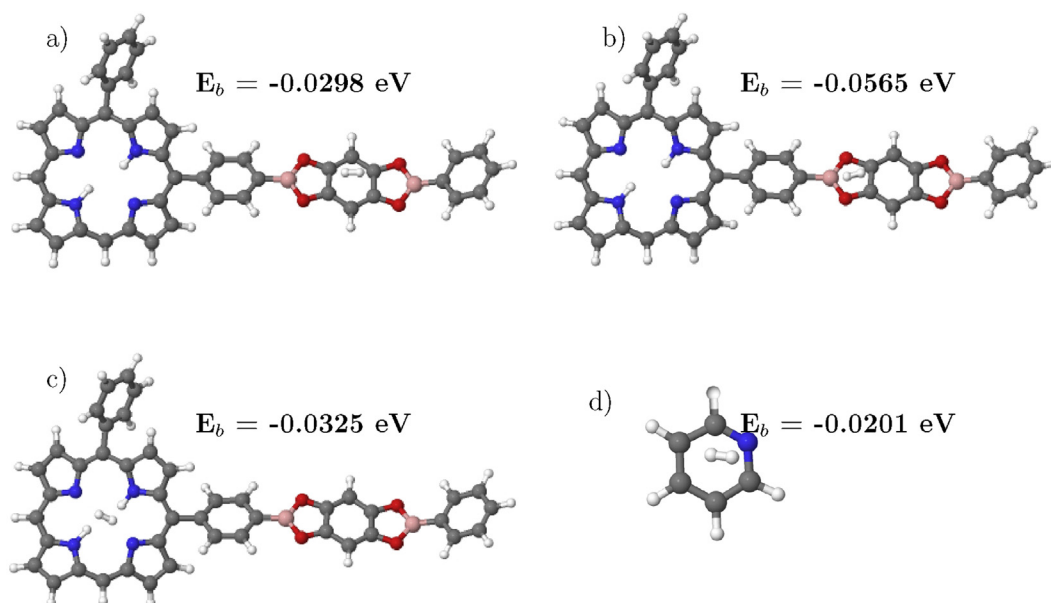


Fig. 4 – Hydrogen adsorption sites and the binding energies (E_b) of H_2 molecule, when the molecule is placed on a) top of one carbon ring, b) top of one boron ring, c) top of porphyrin group and d) top of pyridine molecule. Carbon, oxygen, boron, nitrogen, and hydrogen atoms are shown in grey, red, pink, blue, and white colours, respectively. (For interpretation of the references to color in this figure legend, the reader is referred to the Web version of this article.)

mainly responsible for increasing the interlayer spacing, and hence the accessible volumes for bulk hydrogen adsorption.

Accessible surface area (S_{acc}) and accessible volume (V_{acc}) of COFs for hydrogen molecules were calculated using radical Voronoi tessellation [37,38] as implemented in Zeo++ package [39,40] where a hydrogen gas molecule was rolled over the COF surfaces. Radical Voronoi tessellation is mainly a Monte Carlo sampling approach to calculate probe-accessible surface area and probe-accessible volume by fitting the largest sphere where the Voronoi cell boundaries are defined by the radius. In this method, a radical Voronoi tessellation is performed for a set of spheres centered on each atom (for $i = 1$ to total number of atoms), where the i^{th} sphere has a radius of ($r_{atom_i} + r_{probe}$). Here, for hydrogen molecule, probe diameter of 2.72 Å was used. The calculated pore volumes values are in good agreement with experimental values [9,11,31,41]. The insertion of pyridine molecules significantly increases the accessible volume compared to unmodified COFs. The available volumes for hydrogen adsorption are slightly higher when the pyridine molecules are inserted in each consecutive layer compared to a-bridged doped structures. The calculated properties are tabulated in Table 4.

Radial density profiles of hydrogen molecules from the center of COF were calculated using Eq. (7).

$$\rho(r) = \frac{N}{\pi l [(r + \delta r)^2 - r^2]} \quad (7)$$

where, N is the total number of H_2 molecules present in the cylindrical bin, δr is the bin width, r is the distance from the center of COF and l is the length of cylindrical COF. As a finite length (~ 40 Å) of COFs were used, the whole system was truncated upto l to overcome the system size effect and to

consider infinite long COF. In Fig. 5, the zero value of r represents the center of the COF. The density profiles show the preferential adsorption at surface indicated by a pronounced peak. Fig. 5a represents the density profiles for COF-1. The density peak upto $r < \sim 7$ Å is for the hydrogen molecules which are present inside COF. Afterwards, the density of hydrogen is becoming zero as it is inaccessible due to the presence of COF structure. The isolated tubular arrangement allows outside adsorption and the corresponding layers are formed above $r > \sim 9$ Å. COF-5, shown in Fig. 5b, has higher inside adsorption compared to COF-1 because of higher diameter value. A strong second outer layer is present for COF-1. Due to the small diameter of COF-1, the inner and outer surface of the tubular COF become more curved which slightly increases the overall interaction energy towards the H_2 , compared to large diameter COFs. The small diameter also reduces the inside volume-adsorption, on the other hand, outside surface-adsorption increases. In Fig. 5c, the extended porphyrin group present in H_2 ,P-COF is responsible for the second outer layers. Insertion of pyridine molecules increases the separation distance of each layer. Thus the increased gaps between individual layers become accessible for hydrogen molecules and a non-zero density value is present at ~ 12 Å $> r < \sim 15$ Å in Fig. 5d. The hydrogen molecules were counted by integrating the density profile from $r = 0$ to a certain r value where bulk density reaches, to calculate the absolute number of H_2 molecules adsorbed by the COF (N_{abs}). Excess number of adsorbed hydrogen molecules (N_{ex}) were calculated using Eq. (8).

$$N_{ex} = N_{abs} - \rho_b V_{acc} \quad (8)$$

where, ρ_b is the bulk density of hydrogen gas at the same operating conditions and V_{acc} is the accessible pore volume of adsorbent. Thus N_{ex} defines how much excess hydrogen

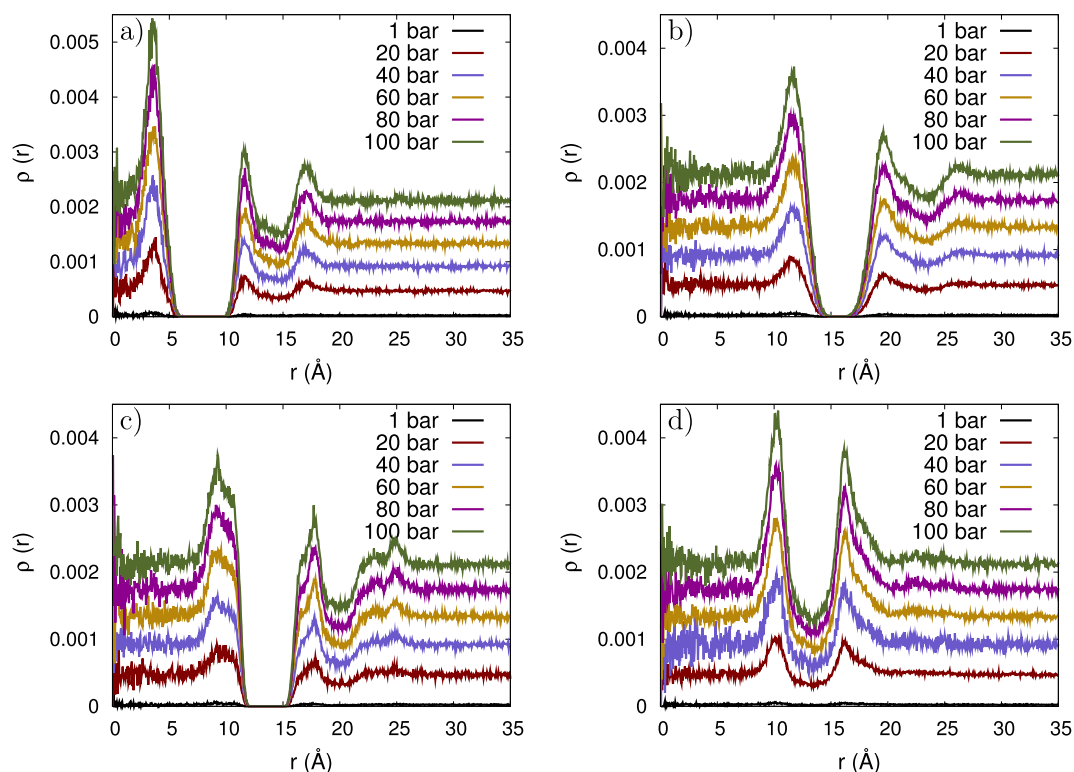


Fig. 5 – Radial density profiles of H₂ from center of COF for a) COF-1, b) COF-5, c) 0-P, H₂-PCOF and d) 1-P, H₂-PCOF at P = 1 bar–100 bar. For rest of the COFs, plots are qualitatively same.

molecules are adsorbed compared to the ideal. Excess adsorptions were calculated in order to have a direct comparison with experimental values. Gravimetric uptake (G) of absolute and excess adsorbed hydrogen molecules were then calculated using Eq. (9). The comparison of excess and absolute adsorption are reported in Supplementary Information [Appendix A].

$$G(\text{wt}\%) = \frac{W_{\text{H}_2}}{W_{\text{H}_2} + W_{\text{COF}}} \times 100 \quad (9)$$

where, W_{H_2} is the total weight of adsorbed hydrogen molecules and W_{COF} is the total weight of COF.

Fig. 6 shows the snapshot of the system containing P-COFs and adsorbed hydrogen as purple spheres at different pressure ranges from 1 bar to 100 bar. The separation distance of two consecutive layers of COF increases with increase in the number of pyridine moiety in the ascending order of 1-P, 2-P, 3-P and 4-P. Higher inter-layer spacing increases the accessible volume of COFs for hydrogen molecules and allows them to access most of the binding states. As the pressure increases from 1 bar to 100 bar, the number of adsorbed hydrogen also increases for all the four types of P-COFs, 1-P, 2-P, 3-P and 4-P. Simulated absolute hydrogen adsorption isotherms were calculated at 298 K and plotted in Fig. 7. Fig. 7a shows the isotherms of pyridine-doped COF where the molecules are doped in each layer whereas, Fig. 7b shows isotherm for alternative layer doped COFs (a-bridged). Pyridine-doped porphyrin-COF structures were compared with un-doped porphyrin-COF and also with COF-1 and COF-

5. Pyridine inserted structures always have higher storage capacities compared to bare COFs. Insertion of pyridine molecules in between COF's layers increases the interlayer spacing and hence, the accessible volume for hydrogen adsorption. At higher pressure, unmodified COFs get saturated where pyridine, P-COFs due to the high available volume still have the capacity to adsorb more hydrogen molecules in their void spaces. Four pyridine molecules doped P-COF (4P, P-COF) has the highest storage capacity and at 100 bar, it has a gravimetric capacity of ~ 5.1 wt%. In comparison with 3D COFs, COF-105 and COF-108 have a hydrogen storage capacity of ~ 4.17 wt% at room temperature and 100 bar [31]. Although the structures are thermodynamically feasible and stable, there might be an issue of stability after hydrogen loading. As the pyridine molecules are bonded to carbon atoms of COF, they are firmly bound as a bridge between two layers. From that perspective, the structures are very tough to break even after hydrogen loading. Insertion of pyridine molecules, on the other hand, increases the inter-layer spacing, thus two parallel porphyrin groups of two layers are far away from each other and have extremely weak van der Waals interactions. The driving force which forms the tubular COF is the weak van der Waals interaction between two layers of COF. The deviation from equilibrium spacing diminishes the non-bonded interactions between layers. Thus the porphyrin groups have the flexibility to be folded in any position around it rather being flat. However, the stability study was not performed due to lack of accurate interaction parameters of COFs. To have a more stable

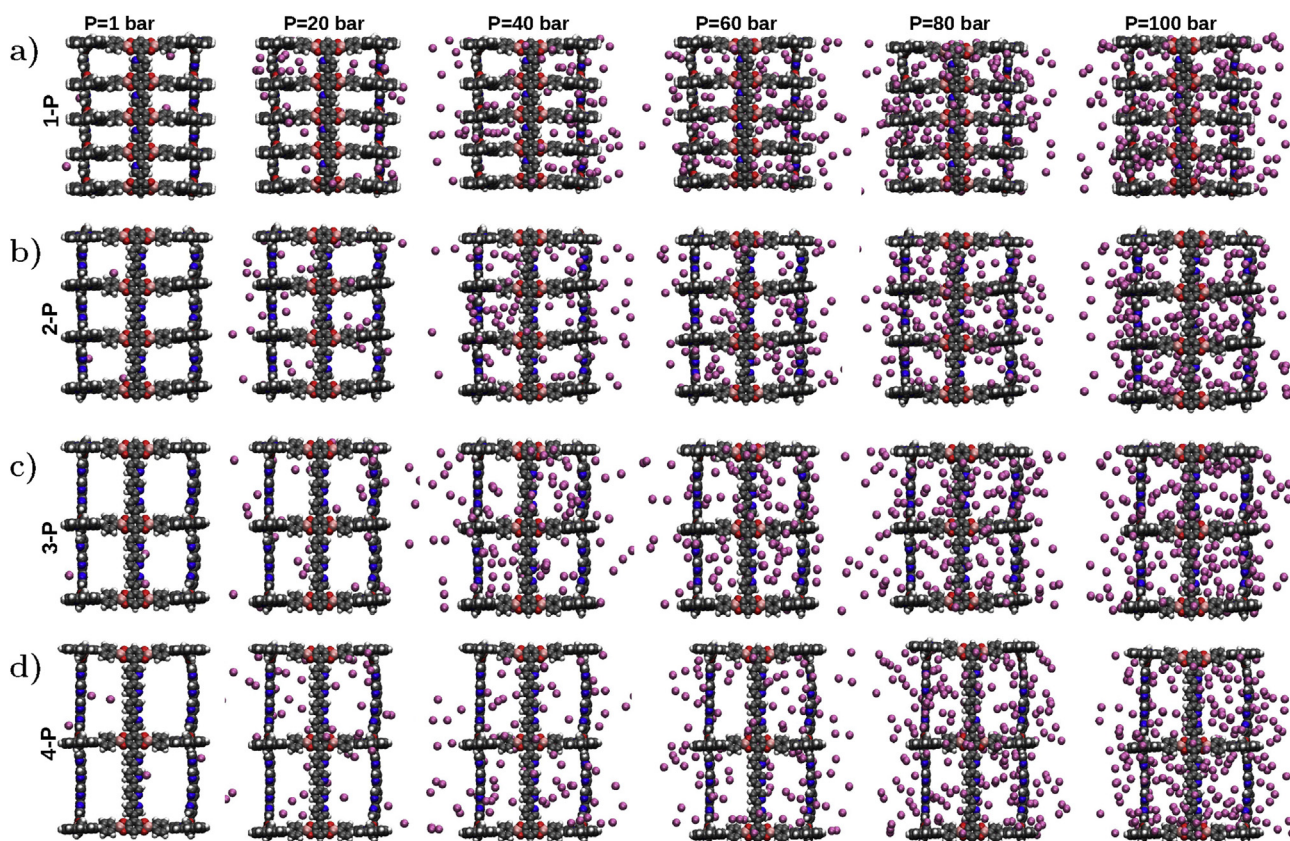


Fig. 6 – The snapshots of hydrogen adsorption in P-COFs at different pressure ranges from 1 to 100 bar, where a) 1-P, H₂-PCOF, b) 2-P, H₂-PCOF, c) 3-P, H₂-PCOF and d) 4-P, H₂-PCOF. Carbon, oxygen, boron and nitrogen atoms are shown in grey, red, pink, and blue colours, respectively. Hydrogen molecules are shown as purple spheres. (For interpretation of the references to color in this figure legend, the reader is referred to the Web version of this article.)

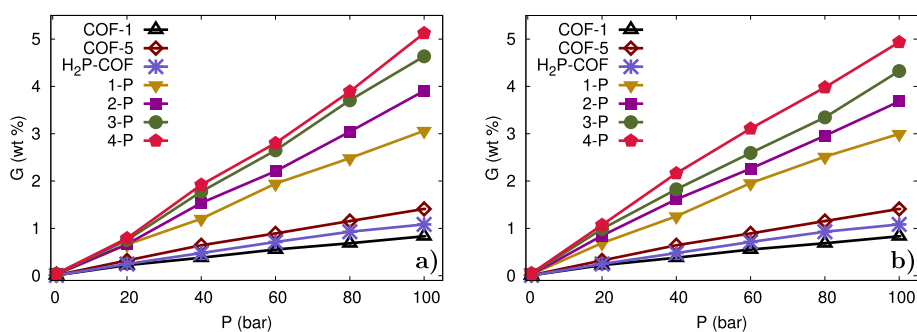


Fig. 7 – Isotherm at 298 K a) where pyridine molecules are bridged to H₂P-COF, b) where pyridine molecules are bridged to alternate layers of H₂P-COF.

structure, next, we inserted the pyridine molecules between two adjacent layers of COFs followed by leaving one next adjacent layer undoped to act as a van der Waals surface, as shown in Fig. 2b and d. Thus, the porphyrin group present in COF will remain as a flat surface even after loading as two parallel porphyrin groups are always separated with equilibrium spacing (~ 3.9 Å). We checked the storage capacities of the a-bridged structures. The free volume slightly decreases due to this specific arrangement which also affects the hydrogen adsorption. The reduced adsorption value is in the deviation range of 0.1 wt% which can easily be neglected

to have more stable adsorption. The study of mechanical stability of the pyridine bridged structures after hydrogen loading can be a further extension of the current study by developing an accurate force-field for COF. In Fig. 8, we plotted hydrogen loading in terms of the mole of adsorbed hydrogen per kg of adsorbent. We evaluated Henry's constant (K_h) by taking the slope of H₂ uptake vs P (Fig. 8), at the low-pressure range (up to 20 bar) where we can assume that the isotherms follow the relation as stated in Eq. (10) [42].

$$H_2 \text{ Uptake} = K_h P \quad (10)$$

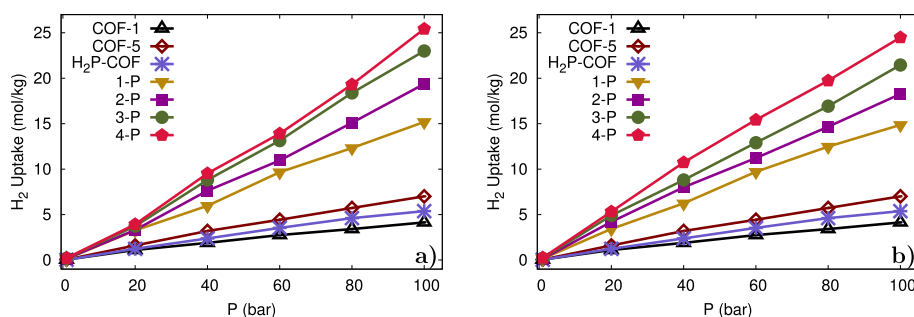


Fig. 8 – Total H₂ uptake in mol/kg at 298 K a) where pyridine molecules are bridged to H₂P-COF, b) where pyridine molecules are bridged to alternate layers of H₂P-COF.

The values of K_h are tabulated in Table 5. By calculating K_h , we can define the strength of the adsorbent. Modified COFs have higher strength of adsorption compared to unmodified COFs. As the number of pyridine molecules (n) used to bridge the COF's layers increases, Henry's constant also monotonously increases. The enhancement in K_h reveals that the pyridine doping increases the strength of the hydrogen adsorption.

The standard storage goal of a material for hydrogen adsorption has both the gravimetric and volumetric terms. Volumetric uptake was calculated using Eq. (11), adapted from the work of Ardelean et al. [43].

$$V_{cap} (g/L) = \rho_{COF} \times \frac{W_{H_2}}{W_{COF}} + \rho_g V_f \quad (11)$$

Where, ρ_{COF} is the accessible void density of COF for H₂ in g/L, $\frac{W_{H_2}}{W_{COF}}$ is g of excess hydrogen/g of COF, ρ_g hydrogen gas density at 298 K and at the respective pressure in g/L and V_f fraction of free volume for H₂. The values of V_f used here are tabulated in Table 4. The predicted volumetric capacities are

Table 5 – Henry's constant of COFs.

COFs (unmodified)	K_h	H ₂ P-COF (bridged)	K_h	H ₂ P-COF (a-bridged)	K_h
COF-1	0.055	1-P	0.163	1-P	0.171
COF-5	0.080	2-P	0.165	2-P	0.209
H ₂ P-COF	0.062	3-P	0.186	3-P	0.245
		4-P	0.196	4-P	0.265

presented in Fig. 9. The volumetric capacity increases with pressure (P) but remains unchanged with the number of doped pyridine moiety (n). Free volume of the material has increased significantly because of the insertion of pyridine moieties. The free volume of P-COF monotonously increases with the number n . All the adsorption sites are also not occupied which is clear from the adsorption isotherm as the saturation has not yet reached. Although the amount of adsorbed hydrogen increases with increase in the number of pyridine moiety, it's almost at the same rate at which the free volume increases. Thus the volumetric capacity plot where the denominator is the free volume of the material, shows constant value for all the P-COFs from 1-P to 4-P. On the other hand, the weight of the material has not increased significantly with increase in n . The material is highly porous and light weight due to which it is possible to reach the gravimetric storage target whereas all of the pores are not filled with hydrogen gas hence has not yet fulfilled the volumetric storage target at this pressure. From the gravimetric and volumetric analysis, we note that the pyridine bridged porphyrin COFs have highest reported uptake at room temperature and 100 bar among all 2D COFs regarding both gravimetric and volumetric capacity (see Table 6). We report a highest hydrogen storage capacity of ~ 5.1 wt% and ~ 20 g H₂/L for tetra-pyridine doped COF which is able to cross the gravimetric DOE target. We compare the performance of the pyridine bridged H₂P-COF at room temperature (298 K) with some commonly used hydrogen adsorbents in Table 6. Widely studied metal organic frameworks (MOFs) have <1 wt% storage capacity at room temperature. Although

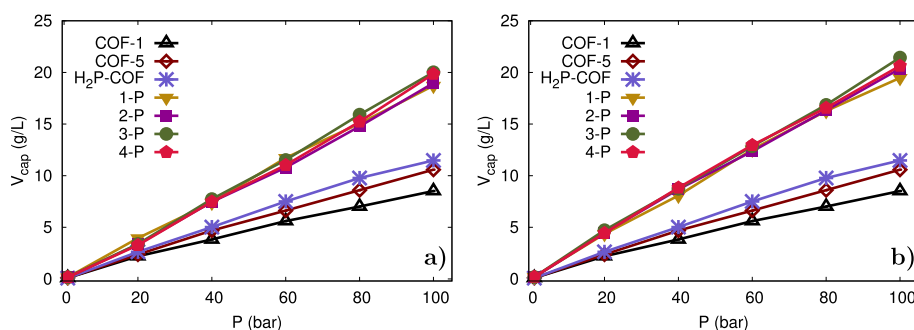


Fig. 9 – Volumetric Capacity of COFs at 298 K a) where pyridine molecules are bridged to H₂P-COF, b) where pyridine molecules are bridged to alternate layers of H₂P-COF.

Table 6 – Reported adsorption capacities of COF-1, COF-5, and some other hydrogen adsorbents.

Material	Operating conditions	G_{cap} (wt%)	V_{cap} (g/L)	Reff
COF-1	77 K and 1 atm	1.28	–	[9]
COF-1	77 K and 35 bar	1.48	–	[11]
COF-1	77 K and 100 bar	3.8	35.8	[10]
COF-5	77 K and 100 bar	5.5	20.5	[10]
COF-1	298 K and 100 bar	0.26	–	[9]
COF-1	298 K and 35 bar	0.04	–	[11]
MOF-5	298 K and 20 bar	1.0	–	[47]
Li–MOF-5	298 K and 1 bar	2.0	–	[45]
Li–MOF-C30	298 K and 100 bar	5.0	–	[44]
Boron nitride nanotubes	298 K and 100 bar	2.6	–	[48]
TiO ₂ nanotube	298 K and 60 bar	2.0	–	[49]
Ti-SWCNT	298 K and 140 bar	2.84	72.95	[5]
Be-SWCNT	298 K and 140 bar	~ 3.5	~70.0	[6]

lithium ion decorated MOFs show promising storage capacity at room temperature [44,45], still the performance is not better than the newly designed H₂P-COF. Boron nitride nanostructures are capable to store <3 wt% at ambient conditions [46]. Titanium and beryllium modified defective single-walled carbon nanotubes (SWCNT) have an ambient storage capacity of <3.5 wt% [5,6]. In comparison with 2D COFs and other similar reported adsorbents (tabulated in Table 6), pyridine doped porphyrin-COFs are the most promising adsorbent for ambient hydrogen storage.

Isosteric heat of adsorption (Q_{st}) is another property which defines the capability of adsorption of the adsorbent and also important to assess the regeneration ability of the adsorbent. It can be calculated using Eq. (12) by measuring how the internal energy (U) is fluctuating due to the fluctuation of the total number of H₂ molecules inside the system.

$$Q_{st} = RT - \frac{\langle UN \rangle - \langle U \rangle \cdot \langle N \rangle}{\langle N^2 \rangle - \langle N \rangle^2} \quad (12)$$

where, R and T are the gas constant and temperature, respectively. Here the symbol $\langle \rangle$ is used to define configuration average. Average value of Q_{st} is plotted with pressure in Fig. 10. The Q_{st} values are not significantly changing with pressure. COF-1 and COF-5 have the highest heat of adsorption which implies they have higher adsorption at low pressure. Although an increasing trend of Q_{st} is observable for modified COF, the change in Q_{st} is very negligible. The

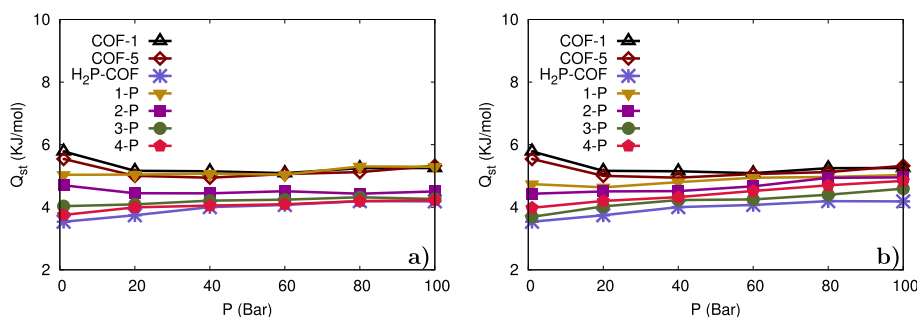


Fig. 10 – Isosteric heat of adsorption (Q_{st}) of COFs at 298 K with pressure a) where pyridine molecules are bridged to H₂P-COF, b) where pyridine molecules are bridged to alternate layers of H₂P-COF.

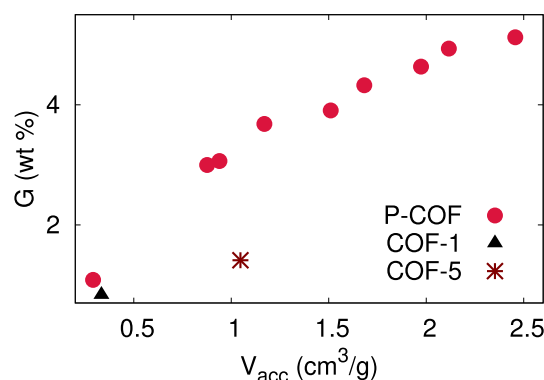


Fig. 11 – Hydrogen loading in terms of gravimetric capacity as a function of free volume of the material.

increasing trend is due to the increase in adsorbate-adsorbent interactions as the hydrogen loading increases. The Q_{st} value is quite low and is also comparable with other hydrogen adsorbents where the value typically varies from 4 to 6 kJ/mol [50,51]. The low value of the heat of adsorption indicates a smooth desorption as less amount of energy is required to regenerate the material. Therefore, Q_s is not playing any major role to increase the adsorption which is also in agreement with the findings of Wang et al. [52] However, our free volume calculations indicate that as the free volume is increasing, the hydrogen adsorption is increasing continuously, as shown in Fig. 11. At the same free volume values, porphyrin COF always has more adsorption. Insertion of pyridine molecules increases the accessible volume of the adsorbent such that the COF structures became a promising material for ambient hydrogen adsorption. Pyridine doping leads to enhance the hydrogen adsorption without much affecting the heat of adsorption and thus, makes it as a promising material for ambient hydrogen adsorption.

Fuel cells are generally operated between 1 and 3 bar of pressure [53]. Adsorbed hydrogen needs to be desorbed at the operating pressure. Thus the hydrogen molecules adsorbed at 100 bar are desorbed at the delivery pressure. To know the amount of accessible hydrogen, desorption pressure of ~5 bar [54] may be used. Here, in order to know the amount of recovered hydrogen, we assumed that the fuel cell is operated at 5 bar and calculated the % recovery by assessing usable hydrogen at 5 bar using the equation below.

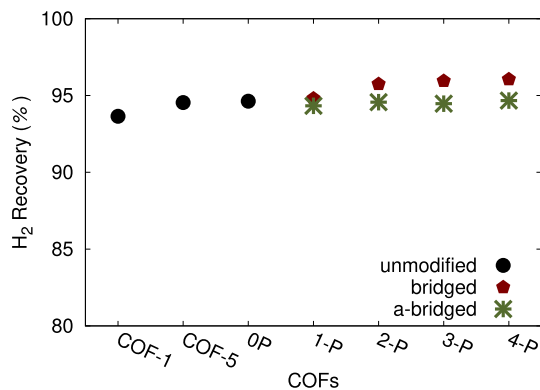


Fig. 12 – Percentage of H₂ recovery adsorbed at 100 bar.

$$H_2 \text{ Usable (wt\%)} = G_{100 \text{ bar}} - G_{5 \text{ bar}} \quad (13a)$$

$$H_2 \text{ Recovery (\%)} = \frac{H_2 \text{ Usable}}{G_{100 \text{ bar}}} \times 100 \quad (13b)$$

where, G stands for the gravimetric capacity and $G_{100 \text{ bar}}$ and $G_{5 \text{ bar}}$ are the capacities at 100 bar and 5 bar, respectively. The % of recovered hydrogen is plotted in Fig. 12. The estimation shows that more than 90% of adsorbed hydrogen molecules are recovered.

Conclusions

A thorough study using DFT and GCMC was carried out for hydrogen adsorption in 2D COFs namely, COF-1, COF-5 and H₂,P-COF. COF-5 has the highest hydrogen adsorption due to its high free volume (2.45 cm³/g) and high binding energy of C₂O₂B ring. Besides, in H₂,P-COF, the porphyrin group increases the adsorption and can easily be further functionalized by transition metals. The 2-D COFs are possible to stack in multiple layers in z direction at equilibrium spacing. In addition, the pyridine molecules, when inserted between two layers of 2-D COFs increases the interlayers spacing and accessible volume for hydrogen adsorption. Consideration of one unit to be stacked in layers gives a cylindrical shape. Formation of tubular COF, increases the effective surface area, and hence the amount of adsorption. A comparison of tubular COFs with the respective planar structures shows a slight variation in adsorption. The tubular arrangement is advantageous where outer surface adsorption is more significant compared to inside volume adsorption. Feasibility of formation and molecular stability of pyridine bridged COF structures were checked by DFT study. To form a more stable structure in the standpoint of physical stability of COFs after hydrogen loading, alternating layers of COF were doped with pyridine molecules. The storage capacity of a-bridged structure is slightly lesser than continuous layer doped structures. Our findings show that tetra pyridine molecule bridged H₂,P-COF has the highest storage capacity among all 2-D COFs. It reached the gravimetric and volumetric uptake of ~5 wt% and 20 gH₂/L, above 2020 gravimetric DOE target and close to the volumetric target (4.5 wt% and 30 g/L), at 298 K and 100 bar.

Acknowledgements

The work was supported by SERB-NPDF-PDF/2017/002495 (Grant No.: SERB/F/6664/2017–2018). The authors thank Computer Center, Indian Institute of Technology Kanpur for providing high performance computational support.

Appendix A. Supplementary data

Supplementary data to this article can be found online at <https://doi.org/10.1016/j.ijhydene.2018.11.066>.

REFERENCES

- [1] Fuel cell technologies office: hydrogen production, Tech. rep. Office of Energy Efficiency and Renewable Energy; 2017. <https://energy.gov/eere/fuelcells/hydrogen-production>.
- [2] Target explanation document: onboard hydrogen storage for light-duty fuel cell vehicles, tech. Rep. Office of Energy Efficiency and Renewable Energy; 2017. <https://energy.gov/eere/fuelcells/downloads/doe-targets-onboard-hydrogen-storage-systems-light-duty-vehicles>.
- [3] Stetson NT. Hydrogen storage program area - plenary presentation. In: 2015 Annual merit review and peer evaluation meeting, fuel cell technologies office. U.S. Department of Energy; 2015.
- [4] Dillon AC, Gennett T, Alleman JL, Jones KM, Parilla PA, Heben MJ. Carbon nanotube materials for hydrogen storage. In: Proc. 2000 U.S. D.O.E. hydrogen program review; 2000.
- [5] Ghosh S, Padmanabhan V. Hydrogen storage in titanium-doped single-walled carbon nanotubes with stone-wales defects. *Diam Relat Mater* 2017;77:46–52.
- [6] Ghosh S, Padmanabhan V. Beryllium-doped single-walled carbon nanotubes with stone-wales defects: a promising material to store hydrogen at room temperature. *Int J Hydrogen Energy* 2017;42(38):24237–46.
- [7] Côté AP, Benin AI, Ockwig NW, O’Keeffe M, Matzger AJ, Yaghi OM. Porous, crystalline, covalent organic frameworks. *Science* 2005;310(5751):1166–70.
- [8] El-Kaderi HM, Hunt JR, Mendoza-Cortés JL, Côté AP, Taylor RE, O’Keeffe M, Yaghi OM. Designed synthesis of 3D covalent organic frameworks. *Science* 2007;316(5822):268–72.
- [9] Li Y, Yang RT. Hydrogen storage in metal-organic and covalent-organic frameworks by spillover. *AIChE J* 2008;54(1):269–79.
- [10] Han SS, Furukawa H, Yaghi OM, Goddard WA. Covalent organic frameworks as exceptional hydrogen storage materials. *J Am Chem Soc* 2008;130(35):11580–1.
- [11] Furukawa H, Yaghi OM. Storage of hydrogen, methane, and carbon dioxide in highly porous covalent organic frameworks for clean energy applications. *J Am Chem Soc* 2009;131(25):8875–83.
- [12] Assfour B, Seifert G. Hydrogen adsorption sites and energies in 2d and 3d covalent organic frameworks. *Chem Phys Lett* 2010;489(1):86–91.
- [13] Wu MM, Wang Q, Sun Q, Jena P, Kawazoe Y. First-principles study of hydrogen adsorption in metal-doped cof-10. *J Chem Phys* 2010;133(15):154706.
- [14] Klontzas E, Tylianakis E, Froudakis GE. Hydrogen storage in lithium-functionalized 3-d covalent-organic framework materials. *J Phys Chem C* 2009;113:21253–7.

- [15] Li F, Zhao J, Johansson B, Sun L. Improving hydrogen storage properties of covalent organic frameworks by substitutional doping. *Int J Hydrogen Energy* 2010;35(1):266–71.
- [16] Mendoza-Cortes JL, Goddard WA, Furukawa H, Yaghi OM. A covalent organic framework that exceeds the DOE 2015 volumetric target for H₂ uptake at 298 K. *J Phys Chem Lett* 2012;3(18):2671–5.
- [17] Kim D, Jung DH, Kim K-H, Guk H, Han SS, Choi K, Choi S-H. Pillared covalent organic frameworks with balanced volumetric and gravimetric hydrogen uptake. *J Phys Chem C* 2012;116(1):1479–84.
- [18] Konda SK, Chen A. Palladium based nanomaterials for enhanced hydrogen spillover and storage. *Mater Today* 2016;19(2):100–8.
- [19] Zhao L, Xu B-Z, Jia J, Wu H-S. A newly designed sc-decorated covalent organic framework: a potential candidate for room-temperature hydrogen storage. *Comput Mater Sci* 2017;137(Supplement C):107–12.
- [20] Kim D, Jung DH, Guk H, Han SS, Park N, Choi K, Choi SH. Theoretical study on porphyrin based covalent organic polyhedra as a hydrogen storage. *Int J Hydrogen Energy* 2013;38(14):6234–40.
- [21] Feng X, Liu L, Honsho Y, Saeki A, Seki S, Irle S, Dong Y, Nagai A, Jiang D. High-rate charge-carrier transport in porphyrin covalent organic frameworks: switching from hole to electron to ambipolar conduction. *Angew Chem Int Ed* 2012;51(11):2618–22.
- [22] Ding S-Y, Gao J, Wang Q, Zhang Y, Song W-G, Su C-Y, Wang W. Construction of covalent organic framework for catalysis: PdCOF-LZU1 in Suzuki–Miyaura coupling reaction. *J Am Chem Soc* 2011;133(49):19816–22.
- [23] Srepusharawoot P, Swatsitang E, Amornkitbamrung V, Pinsook U, Ahuja R. Hydrogen adsorption of Li functionalized covalent organic framework-366: an ab initio study. *Int J Hydrogen Energy* 2013;38(33):14276–80.
- [24] Pachfule P, Kandambeth S, Mallick A, Banerjee R. Hollow tubular porous covalent organic framework (COF) nanostructures. *Chem Commun* 2015;51:11717–20.
- [25] Karak S, Kandambeth S, Biswal BP, Sasmal HS, Kumar S, Pachfule P, Banerjee R. Constructing ultraporos covalent organic frameworks in seconds via an organic terracotta process. *J Am Chem Soc* 2017;139(5):1856–62.
- [26] Tilford RW, Mugavero SJ, Pellechia PJ, Lavigne JJ. Tailoring microporosity in covalent organic frameworks. *Adv Mater* 2008;20(14):2741–6.
- [27] Pardo MA, Perez JM, del Valle MA, Godoy MA, Diaz FR. Pyridine based polymers: synthesis and characterization. *J Chil Chem Soc* 2014;59(2):2464–7.
- [28] Reddy KR, Raghu AV, Jeong HM, Siddaramaiah. Synthesis and characterization of pyridine-based polyurethanes. *Des Monomers Polym* 2009;12(2):109–18.
- [29] Giannozzi P, Baroni S, Bonini N, Calandra M, Car R, Cavazzoni C, Ceresoli D, Chiarotti GL, Cococcioni M, Dabo I, Corso AD, Gironcoli S, Fabris S, Fratesi G, Gebauer R, Gerstmann U, Gougoussis C, Kokalj A, Lazzeri M, Samos LM, Marzari N, Mauri F, Mazzarello R, Paolini S, Pasquarello A, Paulatto L, Sbraccia C, Scandolo S, Sclauzero G, Seitsonen AP, Smogunov A, Umari P, Wentzcovitch RM. QUANTUM ESPRESSO: a modular and open-source software project for quantum simulations of materials. *J Phys Condens Matter* 2009;21(39):395502.
- [30] Plimpton S. Fast parallel algorithms for short-range molecular dynamics. *J Comput Phys* 1995;117(1):1–19.
- [31] Assfour B, Seifert G. Adsorption of hydrogen in covalent organic frameworks: comparison of simulations and experiments. *Microporous Mesoporous Mater* 2010;133(1):59–65.
- [32] Jorgensen WL, Maxwell DS, Tirado-Rives J. Development and testing of the OPLS all-atom force field on conformational energetics and properties of organic liquids. *J Am Chem Soc* 1996;118(45):11225–36.
- [33] Pham T, Forrest KA, Mostrom M, Hunt JR, Furukawa H, Eckert J, Space B. The rotational dynamics of H₂ adsorbed in covalent organic frameworks. *Phys Chem Chem Phys* 2017;19:13075–82.
- [34] Luo J, R. Lloyd, Grand canonical Monte Carlo simulation of hydrogen adsorption in different carbon nanostructures. *Int J Energy a Clean Environ (IJECE)* 10 (1–4).
- [35] Kirklin S, Saal JE, Meredig B, Thompson A, Doak JW, Aykol M, Rühl S, Wolverton C. The open quantum materials database (oqmd): assessing the accuracy of DFT formation energies. *Npj Comput Mater* 2015;1:15010.
- [36] Emery AA, Wolverton C. High-throughput DFT calculations of formation energy, stability and oxygen vacancy formation energy of ABO₃ perovskites. *Sci Data* 2017;4:170153.
- [37] Kerstein AR. Equivalence of the void percolation problem for overlapping spheres and a network problem. *J Phys Math Gen* 1983;16(13):3071.
- [38] van der Marck SC. Network approach to void percolation in a pack of unequal spheres. *Phys Rev Lett* 1996;77:1785–8.
- [39] Willems TF, Rycroft CH, Kazi M, Meza JC, Haranczyk M. Algorithms and tools for high-throughput geometry-based analysis of crystalline porous materials. *Microporous Mesoporous Mater* 2012;149(1):134–41.
- [40] Martin RL, Smit B, Haranczyk M. Addressing challenges of identifying geometrically diverse sets of crystalline porous materials. *J Chem Inf Model* 2012;52(2):308–18.
- [41] Campbell NL, Clowes R, Ritchie LK, Cooper AI. Rapid microwave synthesis and purification of porous covalent organic frameworks. *Chem Mater* 2009;21(2):204–6.
- [42] Bottani EJ, Ismail IMK, Bojan MJ, Steele WA. Henry's law constants and gas-solid potential for CO₂ on graphitized carbon blacks. *Langmuir* 1994;10(10):3805–8.
- [43] Ardelean O, Blanita G, Borodi G, Lazar MD, Misan I, Coldea I, Lupu D. Volumetric hydrogen adsorption capacity of densified MIL-101 monoliths. *Int J Hydrogen Energy* 2013;38(17):7046–55.
- [44] Han SS, Goddard WA. Lithium-doped metal-organic frameworks for reversible H₂ storage at ambient temperature. *J Am Chem Soc* 2007;129(27):8422–3.
- [45] Blomqvist A, Araújo CM, Srepusharawoot P, Ahuja R. Li-decorated metal-organic framework 5: a route to achieving a suitable hydrogen storage medium. *Proc Natl Acad Sci Unit States Am* 2007;104(51):20173–6.
- [46] Fazioğlu E, Yürüm Y, Veziroğlu TN. A review of hydrogen storage systems based on boron and its compounds. *Int J Hydrogen Energy* 2004;29(13):1371–6.
- [47] Rosi NL, Eckert J, Eddaoudi M, Vodak DT, Kim J, O'Keeffe M, Yaghi OM. Hydrogen storage in microporous metal-organic frameworks. *Science* 2003;300(5622):1127–9.
- [48] Ma R, Bando Y, Zhu H, Sato T, Xu C, Wu D. Hydrogen uptake in boron nitride nanotubes at room temperature. *J Am Chem Soc* 2002;124(26):7672–3.
- [49] Lim SH, Luo J, Zhong Z, Ji W, Lin J. Room-temperature hydrogen uptake by TiO₂ nanotubes. *Inorg Chem* 2005;44(12):4124–6.
- [50] Schmitz B, Müller U, Trukhan N, Schubert M, Férey G, Hirscher M. Heat of adsorption for hydrogen in microporous high-surface-area materials. *Chem Phys Chem* 2008;9(15):2181–4.

-
- [51] Zheng Q, Wang X, Gao S. Adsorption equilibrium of hydrogen on graphene sheets and activated carbon. *Cryogenics* 2014;61:143–8.
- [52] Wang L, Wang L, Zhao J, Yan T. Adsorption of selected gases on metal-organic frameworks and covalent organic frameworks: a comparative grand canonical Monte Carlo simulation. *J Appl Phys* 2012;111(11):112628.
- [53] Barbir F. Chapter five - fuel cell operating conditions. In: Barbir F, editor. *PEM fuel cells*. 2nd ed. Boston: Academic Press; 2013. p. 119–57.
- [54] Saldan I, Goslawit-Utke R, Pistidda C, Bösenberg U, Schulze M, Jensen TR, Taube K, Dornheim M, Klassen T. Influence of stoichiometry on the hydrogen sorption behavior in the LiF-MgB₂ system. *J Phys Chem C* 2012;116(12):7010–5.